

Annealing of Heavily Boron-Doped Silicon: Effect on Electrical and Thermoelectric Properties

Laura Zulian*, Francesco Segrado, and Dario Narducci

Università di Milano Bicocca, Dipartimento di Scienza dei Materiali, via R. Cozzi 55, I-20125, Milano, Italy

In previous studies it was shown that heavily boron-doped nanocrystalline silicon submitted to thermal treatments at temperatures ≥ 800 °C is characterized by an anomalously high thermoelectric power factor. Its enhanced performances were ascribed to the formation of SiB_x precipitates at grain boundary, leading to the formation of potential barriers that filter out low-energy carriers, then causing a simultaneous enhancement of the Seebeck coefficient and of the electrical conductivity. To further investigate the effect of thermal treatment on boron-doped nanocrystalline silicon, samples were submitted to a host of annealing processes or of sequences of them at temperatures between 900 and 1000 °C and for various amounts of time. Electrical conductivity and Hall effect measurements were carried out after each thermal treatment over the temperature range 20–300 K. They provided evidence of the formation of an impurity band, and of hopping conduction at very low temperatures. Hall resistivity data versus temperature provided therefore important insights in the electronic structure of the system, which will enable a more complete understanding of the factors ruling energy filtering in this class of materials.

Keywords: Boron, Silicon, Thermoelectric Properties, Nanocrystalline Film, Hall Effect, Electronic Conduction, Hopping.

1. INTRODUCTION

Silicon is the second most abundant element in the Earth's crust, making up roughly one-fourth of its total mass. Also due to its relatively low cost as a semiconductor, it has been the primary material used in the fabrication of devices for integrated circuits as well as for photovoltaics.¹ It is readily available, cheap and has a huge infrastructure and know-how for its production and manipulation. Instead its intrinsic thermoelectric (TE) efficiency is quite poor. However, dimensionally constraints and/or appropriate thermal processes can overcome such limit, driving the material toward interesting figures of merit.² Also physical properties of silicon can be amply modified by playing with the physical chemistry of its impurities and defects.

The energy filtering phenomenon induced by prolonged annealing in highly doped system and its effect on the thermoelectric performances is well known in literature. Already in the 1988, a work by Vining³ showed that the improvement of the TE properties of boron doped nanocrystalline silicon resulting from the precipitation of

a secondary phase of SiB_3 . More recently, Dresselhaus reported examples of enhanced thermoelectric efficiency in nanocrystalline SiGe pellets, possibly due to carrier energy filtering at grain boundaries (GBs).⁴ Similar results were reported also by our research group in a series of papers.^{5–7} We showed that heavily boron doped nanocrystalline silicon submitted to thermal treatments at increasing annealing temperatures beyond 800 °C shows a surprising simultaneous increase of both electrical conductivity and Seebeck coefficient, leading to a power factor as large as 18 mW/mK.² This effect was ascribed to the formation of potential barriers due to the precipitation of a secondary boron-rich phase at grain boundaries, filtering out low energy carriers, and then causing a simultaneous enhancement of the Seebeck coefficient and of the electrical conductivity.⁷

This paper is part of a study aimed at further investigating how annealing processes may affect the thermoelectric properties of heavily boron-doped nanocrystalline silicon thin films. Experimental analyses show that the increase of the material figure of merit achievable through single-shot thermal treatments may be overcome by more complex thermal cycles. However, finding a rationale that may

* Author to whom correspondence should be addressed.

drive preparation strategies is by no mean readily. This paper will actually focus on the analysis of the unusual temperature dependency of the conductivity and of the carrier density observed in the annealed films. Data actually show three different conduction regimes, and the transition temperatures among them is seemingly dependent on the thermal history of the samples. Thus, a proper understanding of the carrier dynamics may be supposed to be needed as a pre-condition to analyze the physical chemistry of boron precipitation, as it might provide clues about the interactions occurring among acceptors in nanocrystalline silicon.

2. EXPERIMENTAL DETAILS

Nanocrystalline silicon films were deposited onto oxidized single crystalline silicon wafers by chemical vapor deposition (CVD) at 610 °C. Films (228 nm thick) were then boron-doped by ion implantation (26 keV, $6 \times 10^{15} \text{ cm}^{-2} + 47 \text{ keV}$, $6 \times 10^{15} \text{ cm}^{-2}$) followed by rapid thermal processing (1050 °C, 20 s). This led to a total nominal boron density of $4.4 \times 10^{20} \text{ cm}^{-3}$. Samples were then submitted to annealing or to sequences of thermal treatments in argon (Table I). Prior to any heat treatment and after it silicon chips were etched using a Piranha solution (H_2SO_4 96% vol.: H_2O_2 30% vol. = 2:1, 95 °C, 30 minutes) to remove organic surface contaminants. Samples were then rinsed in ultrapure deionized water, dried under nitrogen flux, and immersed in DHF (HF 40% vol.: H_2O = 1:10) up to obtaining a fully hydrophobic surface. In addition, samples which underwent a double thermal treatment were submitted to a further BHF etching between the two annealing steps to remove the oxide layer that could have possibly formed.

All samples were characterized by Hall and Seebeck coefficient measurements. Rectangular samples ($0.5 \times 5.2 \text{ cm}^2$) were used to measure Seebeck coefficient by the integral method, setting the temperature of the cold contact at 0 °C while heating the other contact between 40 and 120 °C. Aluminum pads were deposited by evaporation. Contact characteristics were verified to be always linear. Each measurement was carried out in triplicate to assess its reproducibility. Hall measurements were performed on a second set of identical specimens ($1.2 \times 1.2 \text{ cm}^2$) that were contacted according to the Van der Pauw geometry.

Table I. Thermal history of all samples.

Sample	Annealing temperatures		
	900 °C	1000 °C	1000 °C
AG	–	–	–
TT900(2)	2 h	–	–
TT1000(2)	–	2 h	–
TT900(2)1000(2)	2 h	2 h	–
TT1000(2+2)	–	2 h	2 h
TT1000(4)	–	4 h	–

Hall measurements were carried out between 20 K and 300 K with a maximum magnetic field of 0.5 T.

3. RESULTS AND DISCUSSION

3.1. Overview of the Experimental Results

Table II reports the transport coefficients of each sample as obtained by current–voltage characteristics (at 300 K) and Seebeck measurements. As expected, the untreated sample (AG) shows the lower ZT value (0.04), congruent with the expected value for highly doped crystalline silicon (≈ 0.01).⁸ All other samples show instead values of the Seebeck coefficient α larger than 0.40 mV/K. Such a value is a signature of energy filtering due to precipitation of a boron-rich phase at grain boundaries.^{5–7}

All thermal treatments are then functional to increase the thermoelectric performances, although not all to the same extent. Actually the thermal treatment at 900 °C for 2 hours is the least effective while a thermal treatment for the same time but at higher temperatures (1000 °C) leads to a figure of merit of 0.46 at room temperature. Thus, annealing temperature is a crucial parameter to enhance ZT, yet not being the only one. Additional experiments showed actually that the best performances are achieved upon a two-step annealing (2+2 hours) at 1000 °C for which a ZT of 0.61 is achieved. Total annealing time is not however a key factor on itself, as a sample treated for 4 hours (one-step) at 1000 °C shows a much lower ZT. Empirically one would be tempted to conclude that the optimal recipe involve annealing at 1000 °C but also a quenching to room temperature.

3.2. Hall Resistivity and Charge Transport Mechanisms

To get further insights into the experimental data, Hall measurements were performed from 20 and 300 K on all samples after each thermal treatment.⁹

It was immediate to note the striking difference between the resistivity (ρ) trend in treated and untreated samples (Fig. 1). In the as-received sample resistivity shows the temperature dependence typical of metals, with ρ rising with temperature due to the increased carrier scattering. All samples submitted to thermal treatments show instead a different behavior, with a resistivity minimum around 100 K. Above such temperature ρ increases

Table II. Transport parameters of all samples considered in this work.

Sample	Conductivity		Power factor		ZT (T = 300 K)
	$\Omega^{-1} \text{ cm}^{-1}$	α mV/m	mV/K K^2		
AG	532 ± 2	0.14 ± 0.01	0.95 ± 0.51	0.04 ± 0.01	
TT900(2)	200 ± 2	0.41 ± 0.01	4.72 ± 2.01	0.22 ± 0.01	
TT1000(2)	407 ± 3	0.47 ± 0.03	9.82 ± 1.03	0.46 ± 0.01	
TT900(2)1000(2)	189 ± 1	0.62 ± 0.04	11.31 ± 2.04	0.53 ± 0.01	
TT1000(2+2)	225 ± 2	0.67 ± 0.03	13.13 ± 2.08	0.61 ± 0.01	
TT1000(4)	176 ± 1	0.47 ± 0.03	4.78 ± 1.04	0.22 ± 0.01	

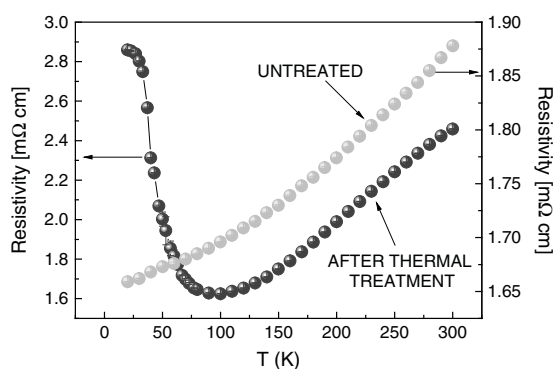


Figure 1. Resistivity versus temperature for typical untreated and thermally treated samples.

with T , as in the case of as grown sample. On the contrary, at lower temperatures, resistivity increases when the temperature decreases, possibly getting to a plateau at ≈ 10 K.

Such a complex behavior may hardly find a rationale in the standard theory of charge transport in lightly doped semiconductors. There, considering that below room temperature the intrinsic carrier contribution may be neglected, electronic conduction is only due to majority carriers (holes for boron-doped silicon). Thus, as the temperature decreases, the carrier concentration in the valence band should rapidly decrease. Therefore, resistivity and the Hall resistance R_H , both proportional to the reciprocal carrier concentration, are predicted to simply increase as temperature decreases.

The actual, typical dependencies of the resistivity and of the Hall resistance upon $1/T$ are displayed in Figure 2. One sees that, differently from what might be expected, the Hall resistance has a maximum at an intermediate temperature while resistivity gets to a plateau in the low temperature limit. Such an anomalous trend was observed for the first time in the Fifties by Hung and Gliemann^{10,11} in heavily doped germanium. It could be explained by assuming that two types of carriers concur to electronic transport, each with its own mobility and scattering mechanism. It is well known¹² that in heavily doped semiconductors, interacting localized states display a broadened distribution of self-energies, and that the overlap of the impurity wave functions may lead to the formation of an impurity band.¹³ Thus, holes may hop from one impurity atom to a close neighbor, and a conduction mechanism inside the impurity band may show up, with mobility μ_H that will be smaller than that of holes drifting into the valence band. However at low temperatures, when the concentration of carriers in the valence band is drastically reduced, the hopping conduction mechanism inside the impurity band is no longer negligible.

On these premises, one may develop a simple model in which both holes in the valence band and in the impurity

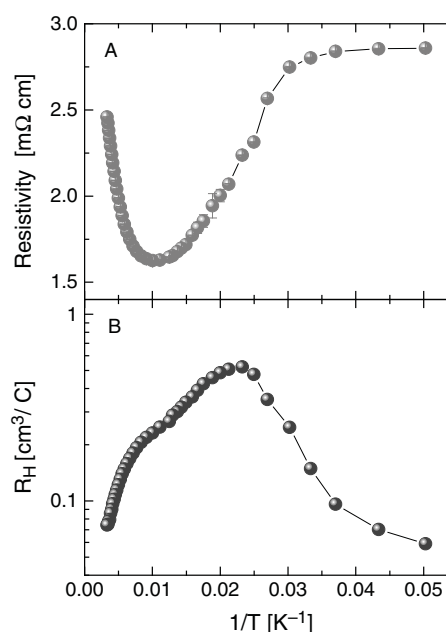


Figure 2. Electrical resistivity (panel A) and Hall resistivity (panel B) for sample TT1000(2) as a function of the reciprocal temperature.

band are taken into account,^{14–17} rewriting the resistivity and the Hall resistance as

$$\frac{1}{\rho} = \frac{1}{p_V e \mu_V} + \frac{1}{p_H e \mu_H} \quad (1)$$

and

$$R_H = r \frac{p_V e \mu_V^2 + p_H e \mu_H^2}{(p_V e \mu_V + p_H e \mu_H)^2} \quad (2)$$

where p_V and p_H are the hole concentrations in the valence and in the impurity band, μ_V and μ_H are the hole mobilities in the valence and in the impurity band, finally r is a numerical factor of the order of unity. Since μ_H is smaller than μ_V , in the limit of high temperature it can be neglected and ρ and R_H revert to the usual formula holding in lightly doped semiconductors. Furthermore, in the high temperature limit all carriers are excited to the valence band, so that $p_H \approx 0$ and

$$R_H \cong \frac{r}{p_V e} \approx \frac{r}{p e} \quad (3)$$

Instead, in the low-temperature limit all carriers will seat in the impurity band, so that $p_V \approx 0$ and

$$R_H \cong \frac{r}{p_H e} \approx \frac{r}{p e} \quad (4)$$

Therefore the Hall resistance at room temperature and at very low temperatures is predicted to take the same value. This is in good agreement with our experiments. As an example, Figure 2 shows that at low temperatures

$R_H = 0.070 \pm 0.002 \text{ cm}^3/\text{C}$ while at room temperature $R_H = 0.074 \pm 0.002 \text{ cm}^3/\text{C}$.

Since the values of the Hall resistance are the same at room temperature and at very low temperatures, and since R_H must increase as the temperature is lowered, then the Hall resistance must pass through a maximum, as observed experimentally. Simple algebra shows that the maximum of the Hall resistance occurs when $p_V e \mu_V = p_h e \mu_h$, namely when the conductivity mechanism switches from valence band to hopping within the impurity band. Figure 3 shows the dependence of R_H on $1/T$. In the saturation range the Hall resistance grows exponentially due to the freezing of the free carrier concentration, while the mobility maintains a high value.

The overall dependency of R_H on T can now be modeled from Eq. (2) when p_V , p_h , μ_V and μ_h are known as a function of temperature. Manifestly enough, p_V is expected to exponentially decrease with $1/T$ in high-medium temperature range; while p_h can be estimated considering that the total number of carriers p is $p = p_V + p_h$. Thus taking μ_V and μ_h as independent of T , μ_V can be obtained from the resistivity at room temperature using $\rho = 1/(p_V e \mu_V) \cong 1/(p e \mu_V)$. For sample TT1000(2) one gets $\mu_V = 30 \text{ cm}^2/\text{Vs}$ while for μ_h it is reasonable to set it to $10 \text{ cm}^2/\text{Vs}$. The comparison between the computed and the experimental values of the Hall resistance are shown in Figure 4. The agreement between the theoretical curve and the data is more than fair.

The same temperature dependence of the Hall resistance has been observed in all the annealed samples save for TT900(2) and TT900(2)1000(2), where a more standard $R_H(T)$ was observed. There the Hall resistance is large at low temperature because nearly all the carriers are in the impurity band and thus none is available for valence band conduction. As the temperature increase the Hall resistance decreases as holes are thermally excited to the valence band. Finally, at the highest temperatures all holes are in the valence band and the Hall resistance changes no more with temperature.

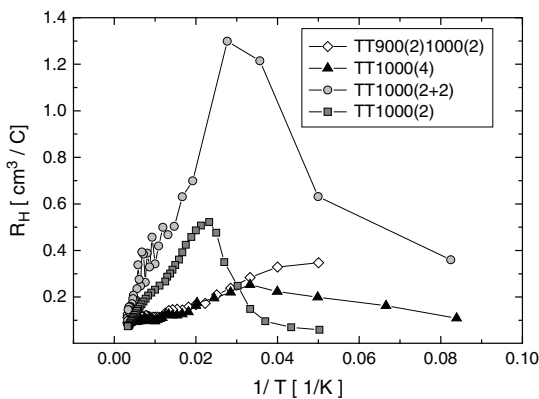


Figure 3. Hall resistivity versus temperature for all investigated samples.

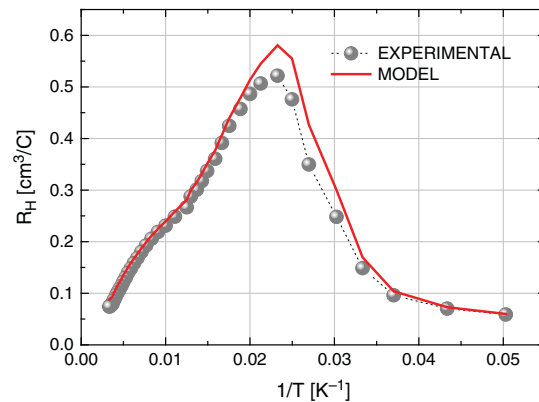


Figure 4. Comparison between measured and computed Hall resistivity. Simulation relies on the assumption of impurity band conduction.

3.3. Electrical Resistivity

Electrical resistivity versus temperature recapitulates the trend described for R_H , confirming that mobility is actually limited by highly screened impurity scattering. Figure 5 shows ρ versus $1/T$ for all the samples under examination. The same qualitative behavior is recognized in all samples. In the high temperature range, all the impurities are ionized and hence the concentration in the band is only slightly dependent upon the temperature. In this range the temperature dependence of the resistivity is essentially dominated by the mobility that is found (as expected) to decrease for increasing temperatures. Resistivity reaches then a minimum at a temperature T_{C1} that actually marks a first transition toward a second conduction regime. In fact a decrease in the temperature causes the gradual freezing of holes, which are partially recaptured by acceptors. In this region, the temperature dependence of ρ is then essentially due to the rapid decrease of the free carrier concentration. If temperature is further decreased silicon enters a regime wherein the main contribution to charge transport comes from holes hopping between occupied to

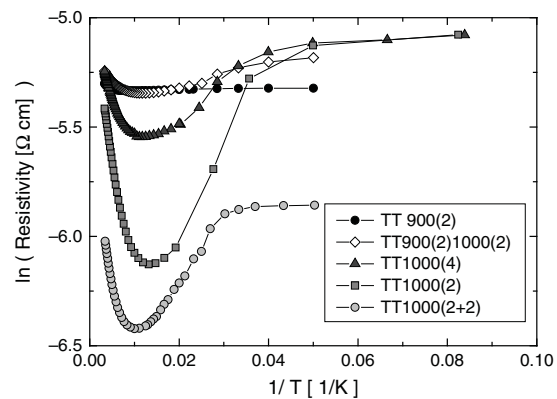


Figure 5. Temperature dependence of resistivity of all investigated samples.

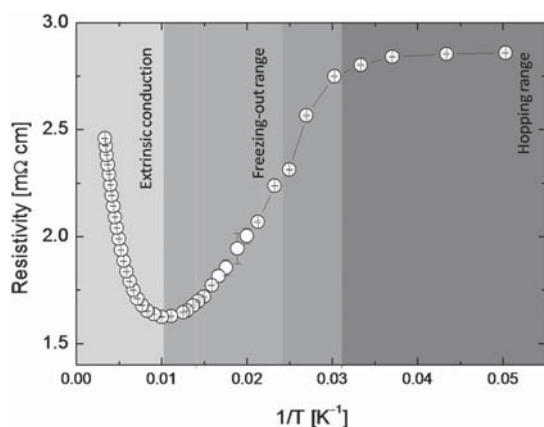


Figure 6. Typical temperature dependence of resistivity. Beside extrinsic conduction, three mechanisms of conduction are observed. Moving from room temperature, a temperature decrease leads to a impurity freezing. A further decrease in temperature causes hopping to be the only contribution to conduction. Note the shoulder marking the transition between freeze-out and hopping regimes, where saturated hopping occurs.

empty levels. Hopping occurs with a very low mobility, in agreement with our measurements.

The two linear regions in the $\ln(\rho)$ versus $1/T$ plot representing the freezing-out and the hopping regimes are separated by a shoulder marking a narrow range of temperatures where resistivity displays a relatively minor dependence on the temperature. Actually, further to band and hopping conduction, heavily doped semiconductors may also display resonant polaronic conduction, namely a charge transport regime due to the resonance between ionized (positively charged) acceptor ions and singly filled (neutral) acceptor levels.^{14–18} Figure 6 summarizes all conduction regimes.

3.4. Transport Regimes and Annealing Processes

A correlation between transport regimes and the annealing samples were submitted to is beyond the aims of this article. Suffice here to note that not only does the transition temperature from the conduction band to the hopping regime T_{C2} change with the annealing conditions, but also that a correlation is found between T_{C2} and the Seebeck coefficient (Table III). This quite suggests that the band structure of the samples does change and reflects the details of the thermal treatment protocol. Since in

Table III. Threshold temperatures as obtained from fit of the resistivity versus $1/T$.

Sample	T_{C1} [K]	T_{C2} [K]
TT900(2)	110	45
TT1000(2)	90	40
TT900(2)1000(2)	80	40
TT1000(2+2)	72	53
TT1000(4)	85	30

degenerate semiconductors the Seebeck coefficient is proportional to the energy derivative of the density of states $g(E)$ at the Fermi energy, it might be speculated that the occurrence of the anomalous simultaneous increase of the electrical conductivity and of the Seebeck coefficient (and the giant value of the power factor) may be correlated to the Fermi level shifting to a region of $g(E)$ where the band tail (due to nanocrystallinity) and the impurity band (due to high doping) overlap, then leading to a large energy derivative of $g(E)$ that coexists with a still large carrier density. Quantitative and more detailed analyses, also encompassing the extent to which the PF increases as a function of annealing temperature, duration, and mode, are however needed to validate such a speculation. It will be addressed in a forthcoming paper.

4. SUMMARY AND CONCLUSIONS

The effect of the annealing on heavily boron-doped nanocrystalline silicon thin film was studied. Since it was known from previous works that annealing at temperature ≥ 800 °C causes the precipitation of a boron-rich second phase, responsible in turn for an increase of the power factor, a host of thermal annealing protocols has been investigated. In this paper we developed a model for the dependency of the Hall resistivity upon the temperature in the cryogenic range. Anomalies in the resistivity and Hall resistance have been actually observed at low temperature. The standard theory for lightly doped semiconductors was insufficient to explain them, and a model accounting for the formation of an impurity band was developed. Three competing conduction mechanisms were recognized, acting over different temperature ranges. Evidence of low-temperature hopping was provided.

Acknowledgment: This work was supported by FP7-NMP-2013-SMALL-7, SiNERGY (Silicon Friendly Materials and Device Solutions for Microenergy Applications) Project, Contract No. 604169.

References and Notes

- G. Fisher, M. R. Seacrist, and R. W. Standley, *Proceedings of the IEEE* 100, 1454 (2012).
- D. Narducci, S. Frabboni, and X. Zianni, *J. Mat. Chem. C* 3, 12176 (2015).
- C. B. Vining, The Thermoelectric Properties of Boron-Doped Silicon and Silicon-Germanium in the As-Hot Pressed Conditions, JPL/Calif. Inst. of Tech. Technical Report (1988).
- S. K. Bux, R. G. Blair, P. K. Gogna, H. Lee, G. Chen, M. S. Dresselhaus, R. B. Kaner, and J.-P. Fleurial, *Adv. Funct. Mat.* 19, 24452452 (2009).
- D. Narducci, E. Selezneva, G. Cerofolini, S. Frabboni, and G. Ottaviani, *J. Sol. State Chem.* 193, 19 (2012).
- D. Narducci, B. Lorenzi, X. Zianni, N. Neophytou, S. Frabboni, G. Gazzadi, A. Roncaglia, and F. Suriano, *Phys. Stat. Sol. A* 211, 1255 (2014).
- N. Neophytou, X. Zianni, H. Kosina, S. Frabboni, B. Lorenzi, and D. Narducci, *Nanotechnology* 24, 205402 (2013).

8. L. Weber and E. Gmelin, *Appl. Phys. A* 53, 136 (1991).
9. D. Long and O. N. Tufte, *The Hall Effect and Its Applications*, edited by C. L. Chien and C. R. Westgate, Springer Science, New York (1980).
10. C. S. Hung and J. R. Gliessman, *Phys. Rev.* 79, 726 (1950).
11. C. S. Hung and J. R. Gliessman, *Phys. Rev.* 96, 1226 (1954).
12. W. Schottky, *Z. Elektrochem.* 45, 33 (1939).
13. H. M. James and A. S. Ginzburg, *J. Phys. Chem.* 57, 840 (1953).
14. H. Frietzche and M. Cuevas, *Phys. Rev.* 119, 1238 (1960).
15. B. I. Shklovskii and A. L. Efros, *Electronic Properties of Doped Semiconductors*, Springer series in Solid State Science, Springer-Verlag, Berlin, Heidelberg (1984), Vol. 45.
16. J. A. Chroboczek, F. H. Pollak, and H. F. Staunton, *Phil. Mag* 50, 113 (1984).
17. T. Chen, K. V. Reich, N. J. Kramer, H. Fu, U. R. Kortshagen, and B. I. Shklovskii, *Nature Materials* 15, 299 (2016).
18. H. Nishimura, *Phys. Rev.* 138, A815 (1965).

Received: 15 March 2016. Accepted: 17 May 2016.